Analytical Derivation of EMF Waveforms in PM Machines based on Permanent Magnet Volume Integration

Maxime R. Dubois
Electrical and Computer Eng. Dept., LEEPCI lab., Université Laval, Québec, CANADA
mrdubois@gel.ulaval.ca

***Abstract*- An analytical expression is developed for predicting emf waveforms resulting from permanent magnets (PM) in electrical machines. The expressions derived in the paper for the flux linkage are based on a volume integral over the PM volume, rather than the usual surface integral over the coil. The proposed method consists in applying a virtual current in the coil of the machine and calculating the magnetic field generated inside the PM volume. The emf waveform is obtained by derivating the flux linkage with respect to time. Analytical expressions of the emf are given for various PM shapes and Halbach magnetization patterns. Experimental verifications of the waveforms obtained are presented in the paper, demonstrating the validity of the expressions obtained theoretically.**

I. INTRODUCTION

Faraday's law implies that the motion of PMs in the vicinity of a coil creates an electromotive force (emf) across that coil. In a PM synchronous machine, the emf generated across each stator coil is an alternative, periodic function of time, with a certain waveform. The harmonic spectrum of the stator waveform will depend on the rotor PM shape and stator winding pattern.

In many applications, predicting the frequency content of the emf and flux waveforms is useful. Such a prediction will enable the machine designer to:

- determine the amplitude of the fundamental emf harmonic component;
- determine the amount of iron losses in the machine related to the flux harmonics;
- optimize the amount of PM material for the desired voltage output.

In past literature, the PM configurations studied were usually simple (e.g. rectangular with radial or parallel magnetization of the PMs). The analytical prediction of the no-load flux density is usually approached by using a scalar or vector potential formulation of the fields in the airgap and solving Laplace's or Poisson's equation with boundary conditions adapted to the geometry analyzed [6][7]. Even with a simple PM structure, the analytical solutions will give long analytical expressions of B_{PM} in the air gap. For more sophisticated PM geometries (see fig. 1), the complexity of the boundary conditions will give rise to significant mathematical difficulties when solving Poisson's or Laplace's equation. In this paper, a different mathematical approach is developed. Analytical expressions will be derived for the emf waveform, which include the time harmonics related to the PM geometry, based on the concept of volumetric flux contribution of PM elements, developed by the author in [1].

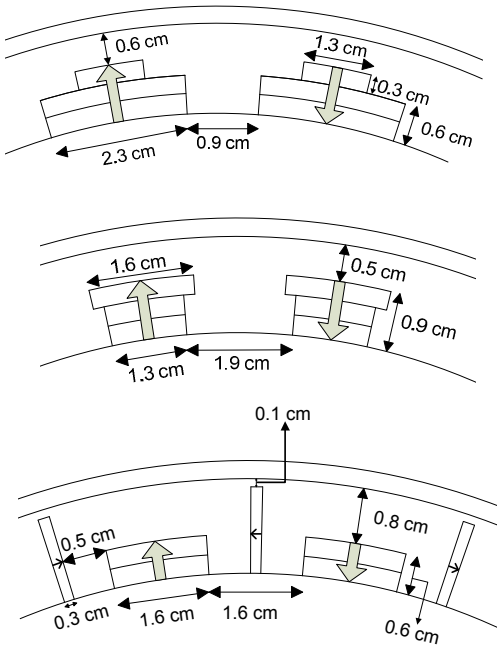

Fig. 1. PM configurations studied in the paper: pyramidal; T-shape; Halbach.

II. ALTERNATE EXPRESSIONS FOR FLUX LINKAGE

In this section, a new expression for the no-load flux linkage λ_{PM} generated by the permanent magnets is presented. Let us assume a fixed stator winding and movable permanent magnets with the arbitrary shapes shown in fig. 2. In the system of fig. 2, we consider a coil made of several turns, where a current is allowed to flow.

We write the product $i\lambda$ "seen" by that coil.

$$i\lambda = \iiint_{Vuniverse} \vec{B} \cdot \vec{H} dv \qquad (1)$$

where λ is the total flux linkage, i.e. created by the PM and the coil. As discussed in [4], $i\lambda$ is the sum of the magnetic energy and magnetic coenergy "seen" by the coil.

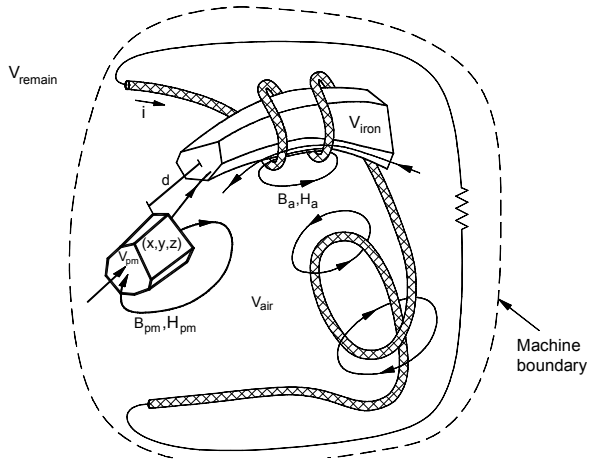

Fig. 2 Generalized PM machine, with arbitrary iron, PM, and coil shapes.

The three variables λ, $\boldsymbol{H}$ and $\boldsymbol{B}$ of (1) have a component created by the current in the coil and a component created by the PMs. In this work, the following assumptions are made:

- PMs have rigid magnetization, that is constant remanent flux density $\boldsymbol{B}_r$ and recoil permeability $\mu_{recoil} = \mu_0$.
- Steel parts are ideal (no saturation and infinite permeability);
- Constant magnetic vector potential throughout the coil conductors cross-section, that is, assumption of filamentary conductors.

The assumptions of linear PM (assumption 1) and ideal iron (assumption 2) allow us to subdivide λ, $\boldsymbol{H}$ and $\boldsymbol{B}$ into λ_a, $\boldsymbol{H}_a$, $\boldsymbol{B}_a$ (component created by the current flowing in the coil, when B_r = 0 T), and λ_{PM}, $\boldsymbol{H}_{PM}$ and $\boldsymbol{B}_{PM}$ (component created by the PM alone, when i = 0). The components $\boldsymbol{H}_a$, $\boldsymbol{B}_a$, $\boldsymbol{H}_{PM}$ and $\boldsymbol{B}_{PM}$ are shown in fig. 2. We rewrite (1):

$$i(\lambda_a + \lambda_{PM}) = \iiint_{V_{universe}} (\bar{B}_a + \bar{B}_{PM}) \cdot (\bar{H}_a + \bar{H}_{PM}) dv \qquad (2)$$

As demonstrated in [5], the integral taken over the universe of the dot product of two vectors is zero, if the curl of the first vector is zero, and the divergence of the second vector is also zero. Since $curl(\boldsymbol{H}_{PM}) = 0$ and $div(\boldsymbol{B}_{PM}) = 0$, (2) becomes:

$$i\lambda_{PM} = \iiint_{V_{universe}} \bar{B}_{PM} \cdot \bar{H}_a dv \qquad (3)$$

With the use of the above stated assumptions, we can easily show (see [1]) that the product of current i and no-load flux linkage λ_{PM} is equal to:

$$i\lambda_{PM} = \iiint_{V_{PM}} \bar{H}_a \cdot \bar{B}_r dv$$

or

$$\lambda_{PM} = \iiint_{V_{PM}} \frac{\bar{H}_a}{i} \cdot \bar{B}_r dv \qquad (4)$$

which reveals that the no-load flux linkage λ_{PM} can be viewed as a volume integral over the volume of all PM material in the machine. At this point, the reader may be uncomfortable with the idea that the no-load flux linkage λ_{PM} can be expressed with (4). However, the demonstration of this equivalence was established in [1] in more detail and will not be entirely repeated here. Experimental results presented in section IV of the present paper will confirm the validity of (4).

As a consequence of (4), we can determine the no-load flux linkage λ_{PM} by injecting a current i in the stator coil, and by calculating the magnetic field $\boldsymbol{H}_a$ created by the stator winding and entering the volume of the PM. Any modification in the magnet geometry will not change the field $\boldsymbol{H}_a$, but will modify the boundary of the volume integral. What was a highly difficult mathematical problem with Laplace's or Poisson's equation can be greatly simplified with eq. (4), provided that the stator winding is a regular geometry.

III. NO-LOAD FLUX LINKAGE IN A SLOTLESS PM MACHINE

In this section, an analytical expression for the emf is derived, based on (4), for the case of a PM machine with a slotless stator with an infinitely thin winding (fig. 3). In the derivation of λ_{PM}, the first step consists in expressing the magnetic field intensity $\boldsymbol{H}_a$ created by the coil, as prescribed by (4). In cylindrical coordinates, the stator-created field is given in [3] for an infinitely thin winding:

$$\frac{H_{ar}}{i} = \sum_{k=1,3,5..}^{\infty} \frac{N_k}{2r} \frac{(r^{2pk} + r_r^{2pk})}{(r_s^{2pk} - r_r^{2pk})} \left[\frac{r_s}{r}\right]^{pk} \cos(pk\alpha) \qquad (5)$$

$$\frac{H_{a\alpha}}{i} = -\sum_{k=1,3,5..}^{\infty} \frac{N_k}{2r} \frac{(r^{2pk} - r_r^{2pk})}{(r_s^{2pk} - r_r^{2pk})} \left[\frac{r_s}{r}\right]^{pk} \sin(pk\alpha) \qquad (6)$$

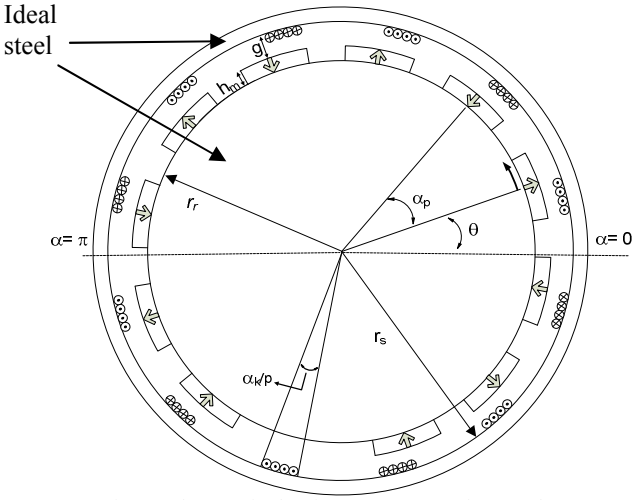

Fig. 3. The PMs in the airgap space. Regular PM shape.

where H_{ar} and $H_{a\alpha}$ are the radial and tangential components of the stator-created magnetic field intensity in cylindrical coordinates and p is the number of pole pairs in the machine. N_k is the coil winding factor for each k^{th} harmonic, r_r and r_s are respectively the rotor and stator radius, and h_m is the magnet thickness.

For one stator coil, the integral volume must extend from radius $r = r_r$ to radius $r = r_r + h_m$, from mechanical angle $\alpha = -\alpha_p/2$ to $\alpha = +\alpha_p/2$, and from axial length $l = 0$ to $l = l_s$. Here we consider that PMs may have the radial and tangential polarization components B_{rr} and $B_{r\alpha}$. For a rectangular PM shape, the tangential component $B_{r\alpha}$ is zero and the PMs are oriented radially. But with a Halbach array, the component $B_{r\alpha}$ will be considered due to the PMs oriented tangentially.

As the cylindrical coordinate system is orthogonal, we may write the dot product of (4) in the following form.

$$\lambda_{PM} = \int_0^{l_s} \int_{r_r}^{r_r+h_m} \int_{-\alpha_p/2}^{+\alpha_p/2} \left(\frac{H_{ar}}{i} B_{rr} + \frac{H_{a\alpha}}{i} B_{r\alpha} \right) r d\alpha dr dl \quad (7)$$

The total emf is obtained by inserting (5) and (6) into (7) and derivating with respect to θ. We obtain:

$$e(\theta) = 2p \frac{d\lambda_{PM}(\theta)}{dt} = 2p \frac{d\lambda_{PM}(\theta)}{d\theta} \frac{d\theta}{dt} = \frac{4\pi p^2 \gamma}{60} \frac{d\lambda_{PM}(\theta)}{d\theta} \quad (8)$$

Eq. (8) assumes that the stator emf is the sum of all the coils individual induced voltages. Inserting (7) into (8) and solving:

$$e(\theta) = -\frac{\pi^2 l_s r_r p \gamma}{60} \sum_{\substack{k=1,3,5... \\ n=k}}^{\infty} \frac{N_k n \sin(n\theta)}{\left[1-\left(\frac{r_r}{r_s}\right)^{pk}\right]\left[1+\left(\frac{r_s}{r_r}\right)^{pk}\right]} \cdot \left[\frac{\left(1+\frac{h_m}{r_r}\right)^{1+pk}-1}{1+pk}\left(B_{rrdn}-B_{r\alpha qn}\right) + \frac{\left(1+\frac{h_m}{r_r}\right)^{1-pk}-1}{1-pk}\left(B_{rrdn}+B_{r\alpha qn}\right) \right] \quad (9)$$

B_{rrdn} and $B_{r\alpha qn}$ are respectively the space harmonic content of the radial PM in the d axis and tangential PM in the q axis. γ is the rotational speed in rpm. The full derivation of (9) is presented in [2].

The analysis can be extended to less conventional PM shapes, consisting of 2 layers of magnets of different widths. In (9), the boundaries of integration were r_r and $r_r + h_m$. For the case of segmented magnets with variable widths for each segment, the integral of (7) will be expressed as a sum of 2 volume integrals, that is, one volume integral for each magnet layer. Only the boundaries need to be changed.

Fig. 4 shows how the decomposition is made. For each magnet layer, a flux linkage (λ_1 for h_{m1} and λ_2 for h_{m2}) and emf are obtained. The total flux linkage is computed by summing λ_1 and λ_2. In our case, the volume has been separated in two regions, but if necessary, it could be done for several regions and the same principle could be used.

Layer 1 goes from $r = r_r$ to $r = r_r + h_{m1}$ and part 2 goes from $r = r_r + h_{m1}$ to $r = r_r + h_m$ where h_{m1} is the height of the first segment.

$$\lambda_{PM} = \lambda_1 + \lambda_2 \quad (10)$$

From eq. (7), we write the flux linkage in each layer.

$$\lambda_1(\theta) = \sum_{\substack{k=1,3,5... \\ n=k}}^{\infty} \frac{\pi N_k \cos(n\theta)}{4p} \int_0^{l_s} \int_{r_r}^{r_r+h_{m1}} \left\{ \frac{r_s^{pk}}{r^{pk}(r_s^{2pk}-r_r^{2pk})} \cdots \right.$$

$$\left. \cdots \left[\left(r^{2pk}+r_r^{2pk}\right) B_{rrdn1} - \left(r^{2pk}-r_r^{2pk}\right) B_{r\alpha qn1} \right] \right\} dr dl \quad (11)$$

$$\lambda_2(\theta) = \sum_{\substack{k=1,3,5... \\ n=k}}^{\infty} \frac{\pi N_k \cos(n\theta)}{4p} \int_0^{l_s} \int_{r_r+h_{m1}}^{r_r+h_m} \left\{ \frac{r_s^{pk}}{r^{pk}(r_s^{2pk}-r_r^{2pk})} \cdots \right.$$

$$\left. \cdots \left[\left(r^{2pk}+r_r^{2pk}\right) B_{rrdn2} - \left(r^{2pk}-r_r^{2pk}\right) B_{r\alpha qn2} \right] \right\} dr dl \quad (12)$$

The space harmonics B_{rrdn} and $B_{r\alpha qn}$ are identified with indices 1 and 2, because the radial and tangential space harmonics of layer 1 may be different from that of layer 2. Eq. (11) and (12) are solved as follows:

$$\lambda_1(\theta) = \frac{\pi l_s r_r}{4p} \sum_{\substack{k=1,3,5... \\ n=k}}^{\infty} \frac{N_k \cos(n\theta)}{\left[1-\left(\frac{r_r}{r_s}\right)^{pk}\right]\left[1+\left(\frac{r_s}{r_r}\right)^{pk}\right]} \cdot \left[\frac{\left(1+h_{m1}/r_r\right)^{1+pk}-1}{1+pk}\left(B_{rrdn1}-B_{r\alpha qn1}\right) + \frac{\left(1+h_{m1}/r_r\right)^{1-pk}-1}{1-pk}\left(B_{rrdn1}+B_{r\alpha qn1}\right) \right] \quad (13)$$

$$\lambda_2(\theta) = \frac{\pi l_s r_r}{4p} \sum_{\substack{k=1,3,5... \\ n=k}}^{\infty} \frac{N_k \cos(n\theta)}{\left[1-\left(\frac{r_r}{r_s}\right)^{pk}\right]\left[1+\left(\frac{r_s}{r_r}\right)^{pk}\right]} \cdot \left[\frac{\left(1+h_m/r_r\right)^{1+pk}-\left(1+h_{m1}/r_r\right)^{1+pk}}{1+pk}\left(B_{rrdn2}-B_{r\alpha qn2}\right) + \frac{\left(1+h_m/r_r\right)^{1-pk}-\left(1+h_{m1}/r_r\right)^{1-pk}}{1-pk}\left(B_{rrdn2}+B_{r\alpha qn2}\right) \right] \quad (14)$$

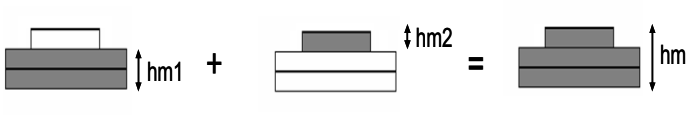

Fig 4. PM integration volume

The emf is obtained by derivating (13) and (14) with respect to θ. We obtain:

$$e(\theta) = e_1(\theta) + e_2(\theta) \tag{15}$$

where

$$e_1(\theta) = -\frac{\pi^2 l_s r_r p \gamma}{60} \sum_{\substack{k=1,3,5... \\ n=k}}^{\infty} \frac{N_k n \sin(n\theta)}{\left[1-\left(\frac{r_r}{r_s}\right)^{pk}\right]\left[1+\left(\frac{r_s}{r_r}\right)^{pk}\right]}$$

$$\cdot\left[\frac{\left(1+h_{m1}/r_r\right)^{1+pk}-1}{1+pk}\left(B_{rrdn1}-B_{r\alpha qn1}\right)+\frac{\left(1+h_{m1}/r_r\right)^{1-pk}-1}{1-pk}\left(B_{rrdn1}+B_{r\alpha qn1}\right)\right] \tag{16}$$

$$e_2(\theta) = -\frac{\pi^2 l_s r_r p \gamma}{60} \sum_{\substack{k=1,3,5... \\ n=k}}^{\infty} \frac{N_k n \sin(n\theta)}{\left[1-\left(\frac{r_r}{r_s}\right)^{pk}\right]\left[1+\left(\frac{r_s}{r_r}\right)^{pk}\right]}$$

$$\cdot\left[\frac{\left(1+h_m/r_r\right)^{1+pk}-\left(1+h_{m1}/r_r\right)^{1+pk}}{1+pk}\left(B_{rrdn2}-B_{r\alpha qn2}\right)\right.$$

$$\left.+\frac{\left(1+h_m/r_r\right)^{1-pk}-\left(1+h_{m1}/r_r\right)^{1-pk}}{1-pk}\left(B_{rrdn2}+B_{r\alpha qn2}\right)\right] \tag{17}$$

IV. Experimental Results

In this section, four magnet geometries are illustrated:

- Rectangular – 1 layer – radial magnetization
- Pyramidal – 2 layers – radial magnetization
- T-shape – 2 layers – radial magnetization
- Halbach – 2 layers – radial and tangential magnetizations

For each configuration, the space harmonics of the remanent flux densities B_{rrdn} and $B_{r\alpha qn}$ are illustrated, with the emf waveform calculated with eq. (15), (16) and (17). For each configuration, a rotor and stator were built and the emf waveform was measured with an oscilloscope, across 1 coil made of 5 turns, as shown in fig. 5.

The parameters of each configuration are given in Table I.

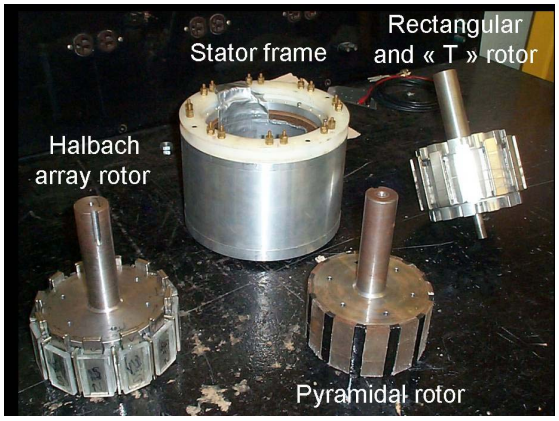

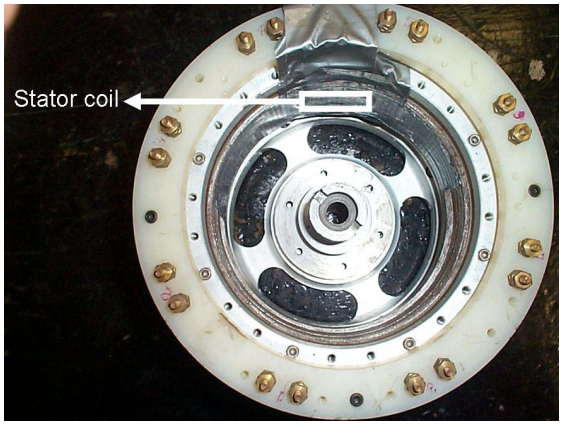

Fig. 5. Experimental machine.

TABLE I : GEOMETRICAL PARAMETERS OF THE 4 ROTOR CONFIGURATIONS

Parameters	Symbol	Rectangular	Pyramidal	"T"	Halbach	Units [a]
Pole number	2p	12	12	12	12	—
Winding	-	Full-pitch	Full-pitch	Full-pitch	Full-pitch	
Number of turns per coil	N / 2p	5	5	5	5	—
Rotor radius	r_r	0.061	0.060	0.061	0.061	m
Stator radius	r_s	0.075	0.075	0.075	0.075	m
Airgap thickness	g	5	6	5	8.2 (radial) 1.2 (tangent)	mm
Radial thickness	h_m	9	9	9	6 (radial) 13 (tangent)	mm
Magnets Electrical arc	–	73	132 (base) 73 (top)	73 (base) 90 (top)	90 (radial) 13 (tangent)	°
Coil width	α_k	2.3	2.3	2.3	2.3	°
Pole-pitch	α_p	30	30	30	30	°
Magnet remanence	B_r	1.15	1.15	1.15	1.15	T
Coil length	l_s	20	20	20	20	mm
Coil width	—	39.3	39.3	39.3	39.3	mm
Rotational speed	γ	1462	733	1355	1345	rpm

The experimental emf waveforms are illustrated in fig. 6c), 7c), 8c), 9c) and compared with the theoretical waveforms on the same figure. For a rectangular magnet shape with radial magnetization, fig. 6 shows the magnet configuration, the spectral content of the remanent flux density in the radial direction B_{rrdn} and the experimental and theoretical emf waveforms. The results presented in fig. 6 indicate good agreement between the theoretical waveform obtained with eq. (9) and the experimental waveform.

In fig. 7 and 8, two-layer magnet configurations are considered, with a pyramidal stack of magnets and a T configuration. The results presented in fig. 7 and 8 indicate a good agreement between the theoretical waveforms obtained with eq. (13), (14), (15) and the experimental waveforms.

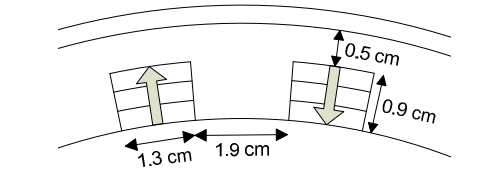

a)

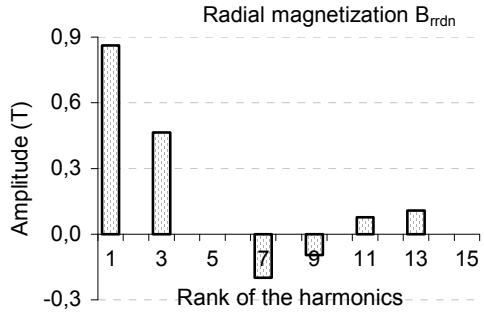

b)

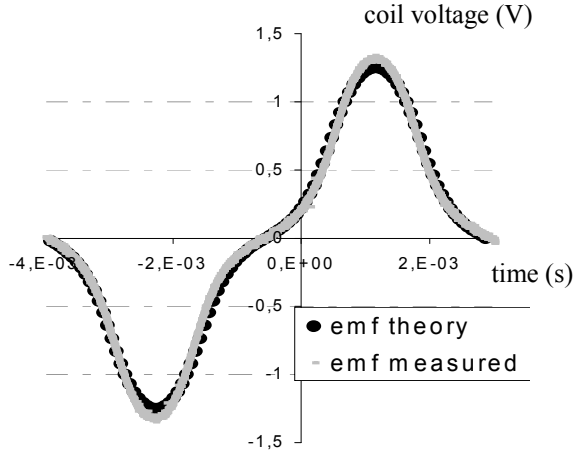

c)

Fig. 6. Results with the rectangular shape. a) magnet configuration, b) space harmonics of the PM magnetization, c) experimental and theoretical voltage waveforms at no-load across one coil of 5 turns.

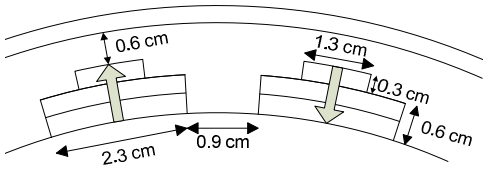

a)

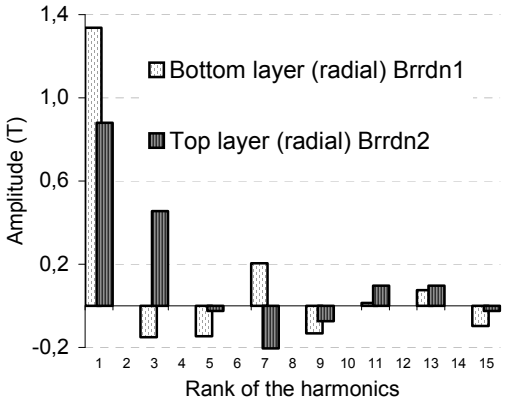

b)

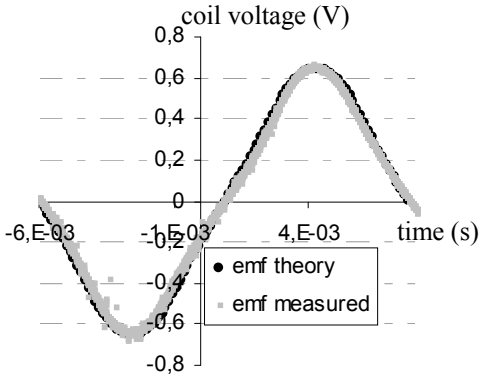

c)

Fig. 7. Results with the pyramidal shape. a) magnet configuration, b) space harmonics of the PM magnetization, c) experimental and theoretical voltage waveforms at no-load across one coil of 5 turns.

In fig. 9, a new characteristic is present that is not found on the other figures: the tangential component. In the Halbach array of fig. 9, both components of B_r, radial and tangential are presented. On the upper layer of the PM arrangement of fig. 9a), only tangential PMs are present. For that upper magnet layer, the PM space harmonic content considered is the tangential harmonic content $B_{r\alpha n}$ only, and the radial harmonic content is zero for all B_{rrn}. The results presented in fig. 9 also indicate good agreement between the theoretical waveform obtained with eq. (13), (14), (15) and the experimental waveform.

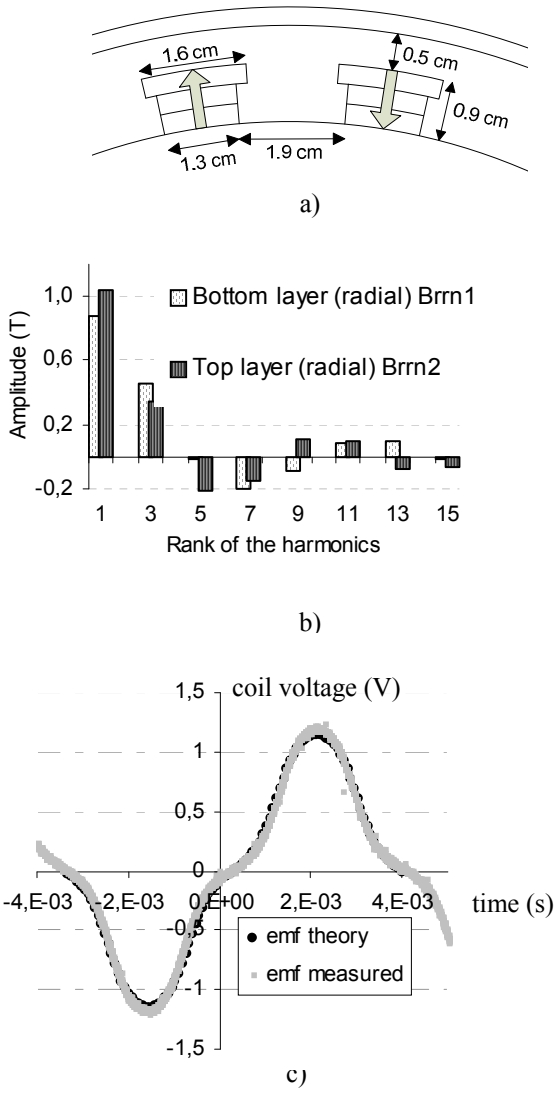

Fig. 9. Results with the "T" shape. a) magnet configuration, b) space harmonics of the PM magnetization, c) experimental and theoretical voltage waveforms at no-load across one coil of 5 turns.

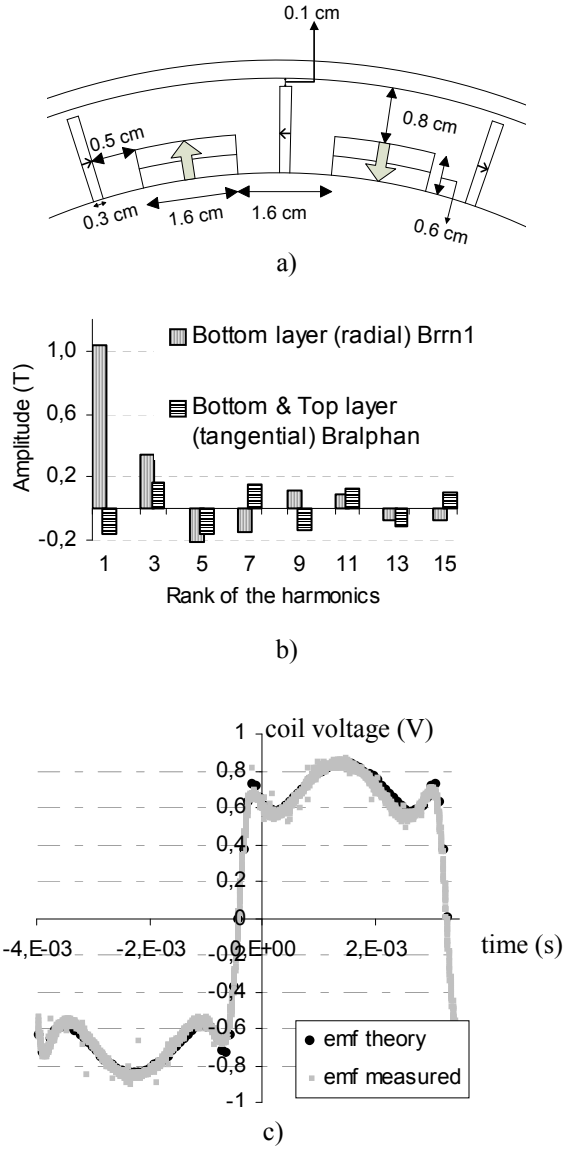

Fig. 10. Results with the Halbach array. a) magnet configuration, b) space harmonics of the PM magnetization, c) experimental and theoretical voltage waveforms at no-load across one coil of 5 turns.

V. Conclusion

The paper has presented an innovative method for deriving the no-load flux linkage and emf in a permanent magnet machine, by performing a volume integral on the magnets. The method was applied to a cylindrical PM machine with surface magnets, with various magnet configurations. Analytical expressions were obtained, which predict the emf and no-load flux waveforms very accurately. The waveforms were validated experimentally on four configurations of PMs on the rotor: a rectangular magnet configuration, a pyramidal configuration, a T configuration and a two-layer Halbach array. In each case, the waveform obtained experimentally was closely matched by the theoretical waveform.

References

[1] M.R. Dubois, H. Polinder, and J. A. Ferreira, "Contribution of permanent magnet volume elements to the no-load voltage in machines," *IEEE Trans. Magnetics*, vol. 36, pp. 1784-1792, May 2003.

[2] M.R. Dubois, and G. Mailloux, "Analytical Calculation of No-load Voltage Waveforms in Machines Based on Permanent Magnet Volume Integration," *IEEE Trans. Magnetics*, vol. 44, pp. 581-589, May 2008.

[3] H. Polinder, On the losses in a high-speed permanent-magnet generator with rectifier, Ph.D. dissertation, Delft Univ. Tech., Delft, The Netherlands, 1998.

[4] O. K. Mawardi, "On the concept of coenergy" Journal of Franklin Institute, vol. 264, no. 1, pp. 313-332, 1957.

[5] W. F. Brown, Magnetostatic Principles in Ferromagnetism, North-Holland, Amsterdam 1962.

[6] Z.Q. Zhu, D. Howe, and B. Ackermann, "Instantaneous magnetic field distribution in brushless permanent magnet dc motors, part I: open-circuit field," IEEE Trans. Magn., vol. 29, no. 1, pp. 124-135, Jan. 1993.

[7] N.Boules, "Two-dimensional field analysis of cylindrical machines with permanent magnet excitation," IEEE Trans. Ind. Appl., vol. IA-20, no. 5, pp. 1267-1277, Sept./Oct. 1984.